

A scattering phantom for observing long range order with two-dimensional angle-resolved Low-Coherence Interferometry

Steven K. Yarmoska, Sanghoon Kim, Thomas E. Matthews and Adam Wax*

*Department of Biomedical Engineering and Fitzpatrick Institute for Photonics,
Duke University, Durham NC 27708, USA*

**mailto:a.wax@duke.edu*

Abstract: Angle-resolved low coherence interferometry (a/LCI) is an approach for assessing tissue structure based on light scattering data. Recent advances in a/LCI have extended the analysis to study scattering distributions in two dimensions. In order to provide suitable scattering phantoms for 2D a/LCI, we have developed phantoms based on soft lithography which can provide a range of structures including long range order. Here we characterize these phantoms and demonstrate their utility for providing standardized multi-scale structural information for light scattering measurements.

©2013 Optical Society of America

OCIS codes: (290.0290) Scattering; (290.3200) Inverse scattering; (290.5820) Scattering measurements; (120.3180) Interferometry.

References and Links

1. A. Wax, C. H. Yang, V. Backman, K. Badizadegan, C. W. Boone, R. R. Dasari, and M. S. Feld, "Cellular organization and substructure measured using angle-resolved low-coherence interferometry," *Biophys. J.* **82**(4), 2256–2264 (2002).
 2. Y. Zhu, N. G. Terry, J. T. Woosley, N. J. Shaheen, and A. Wax, "Design and validation of an angle-resolved low-coherence interferometry fiber probe for in vivo clinical measurements of depth-resolved nuclear morphology," *J. Biomed. Opt.* **16**(1), 011003 (2011).
 3. N. Terry, Y. Zhu, J. K. M. Thacker, J. Migaly, C. Guy, C. R. Mantyh, and A. Wax, "Detection of intestinal dysplasia using angle-resolved low coherence interferometry," *J. Biomed. Opt.* **16**(10), 106002 (2011).
 4. J. W. Pyhtila, K. J. Chalut, J. D. Boyer, J. Keener, T. D'Amico, M. Gottfried, F. Gress, and A. Wax, "In situ detection of nuclear atypia in Barrett's esophagus by using angle-resolved low-coherence interferometry," *Gastrointest. Endosc.* **65**(3), 487–491 (2007).
 5. N. G. Terry, Y. Zhu, M. T. Rinehart, W. J. Brown, S. C. Gebhart, S. Bright, E. Carretta, C. G. Ziefle, M. Panjehpour, J. Galanko, R. D. Madanick, E. S. Dellon, D. Trembath, A. Bennett, J. R. Goldblum, B. F. Overholt, J. T. Woosley, N. J. Shaheen, and A. Wax, "Detection of Dysplasia in Barrett's Esophagus With In Vivo Depth-Resolved Nuclear Morphology Measurements," *Gastroenterology* **140**(1), 42–50 (2011).
 6. J. P. Bouchard, I. Noiseux, I. Veilleux, and O. Mermut, "The role of optical tissue phantom in verification and validation of medical imaging devices," in *BioPhotonics*, 2011 International Workshop on. (2011).
 7. H. J. van Staveren, C. J. Moes, J. van Marie, S. A. Prahl, and M. J. van Gemert, "Light scattering in Intralipid-10% in the wavelength range of 400-1100 nm," *Appl. Opt.* **30**(31), 4507–4514 (1991).
 8. J. R. Mourant, T. Fuselier, J. Boyer, T. M. Johnson, and I. J. Bigio, "Predictions and measurements of scattering and absorption over broad wavelength ranges in tissue phantoms," *Appl. Opt.* **36**(4), 949–957 (1997).
 9. D. Wang, Y. Chen, and J. T. C. Liu, "A liquid optical phantom with tissue-like heterogeneities for confocal microscopy," *Biomed. Opt. Express* **3**(12), 3153–3160 (2012).
 10. A. Agrawal, T. J. Pfefer, N. Gilani, and R. Drezek, "Three-dimensional characterization of optical coherence tomography point spread functions with a nanoparticle-embedded phantom," *Opt. Lett.* **35**(13), 2269–2271 (2010).
 11. Y. L. Kim, Y. Liu, R. K. Wali, H. K. Roy, and V. Backman, "Low-coherent backscattering spectroscopy for tissue characterization," *Appl. Opt.* **44**(3), 366–377 (2005).
 12. M. Giacomelli, Y. Zhu, J. Lee, and A. Wax, "Size and shape determination of spheroidal scatterers using two-dimensional angle resolved scattering," *Opt. Express* **18**(14), 14616–14626 (2010).
 13. J. W. Pyhtila, H. Ma, A. J. Simnick, A. Chilkoti, and A. Wax, "Analysis of long range correlations due to coherent light scattering from in-vitro cell arrays using angle-resolved low coherence interferometry," *J. Biomed. Opt.* **11**(3), 034022 (2006).
-

1. Introduction

Angle-resolved low-coherence interferometry (a/LCI) is a light scattering technique that combines angle-resolved measurements with the depth resolution achieved by using a broadband source in an interferometry scheme. The light scattering data may then be analyzed to assess structural features. For example, a/LCI has demonstrated the ability to accurately determine the average size and refractive index of biological scatterers, such as the nuclei of epithelial cells [1]. Further development of a/LCI has led to a fiber optic implementation that is compatible with the standard accessory channel of most endoscopes [2]. This system has been applied to detect pre-cancerous cells in epithelial tissues [3, 4]. Recent application in a clinical study of Barrett's esophagus patients has shown that it can distinguish between normal and dysplastic tissues *in vivo* with high sensitivity and specificity [5].

With much recent interest in the use of optical techniques for biomedical applications, the need for scattering standards has become important, especially for translation of such biophotonics techniques for clinical use [6]. Many techniques are validated using Intralipid [7] or polystyrene microspheres [8], or combinations of these [9] for their ability to provide optical properties similar to tissues. One drawback of these methods arises from the use of liquid-based phantoms which often require time averaging to mitigate the effects of speckle. This effect can be overcome by the use of solid phantoms [10–12] which freeze the optical scatterers in specific locations and thus exchange a time-varying speckle pattern for a static one. The static speckle pattern can be analyzed to determine the relative spacing of scattering objects, the goal of the phantom development presented here. In addition, liquid phantoms are typically limited to containing scatterers on the order of 10 microns or less and thus, cannot capture the overall long range order that is often seen in epithelial tissues which can be modulated due to the presence of disease. To address this need, we seek to create phantoms with regular arrays of scattering features.

2. Methods

a. Two dimensional (2D) a/LCI

We recently advanced a/LCI to permit measurements over two scattering directions, providing more detailed information about scattering structures [12]. In the original a/LCI implementations, scattered light is detected in a single scattering plane (1D a/LCI). However, when analyzing anisotropic structures, such as spheroids, the scattering distribution will change significantly as a function of not only polar angle (θ), as would be the case for spherically symmetric scatterers, but will also exhibit non-trivial dependence on azimuth (ϕ) relative to the incident polarization. In the first implementation of 2D a/LCI, a spectral domain low coherence interferometer was constructed where the signal field was collected by scanning a single mode fiber across a conjugate Fourier plane of the sample, effectively creating a raster scan of the 2D (θ, ϕ) angular scattering distribution (Fig. 1). The scan time was approximately 12 minutes which would likely preclude clinical utility. To overcome this limitation, we have constructed a new 2D a/LCI system (Fig. 1) in which the scattering field is overlapped with a reference field and the conjugate Fourier plane is made to coincide with the entrance slit of an imaging spectrometer (Princeton Instruments, SP-2150) The spectrometer has a 150 mm focal length and uses a 600 lp/mm grating. The sensor is a Pike F-032 camera (AVT). With the parallel acquisition method, the scan time at one scattering plane (θ_1 , horizontal direction in Fig. 1) takes less than 1 ms, and with 550 angular scans (θ_2 , vertical direction in Fig. 1), total acquisition time for entire scattering field takes approximately 200 ms. The angular resolution of 1 mrad will dictate the maximum correlation range that can be measured to 450 μm through the Fourier transform (FT) relationship, but in practice the beam diameter will limit the maximum correlation distance. The angular range achieved here of 0.55 rad (31°) will place a limit on the smallest detectable correlation distance of approximately 1.5 μm .

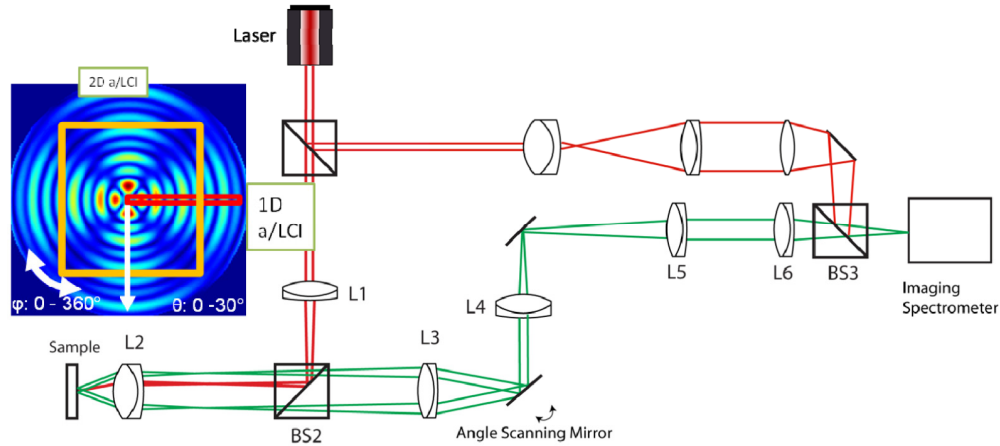


Fig. 1. (Inset) Comparison of 1D and 2D a/LCI measurements superimposed on a typical scattering pattern, given as field amplitude. (Main) New 2D a/LCI system schematic. Light from Ti:Sapphire laser ($\lambda = 830 \text{ nm}$ $\Delta\lambda = 17 \text{ nm}$) is split into an input to the sample and a reference beam (red). Light scattered by the sample (green) is imaged onto the entrance slit of the spectrometer, located in a conjugate Fourier plane. By including an angle scanning mirror between L3 and L4, light in different scattering planes is made to overlap the entrance slit such that the scattering across the 2D plane can be measured.

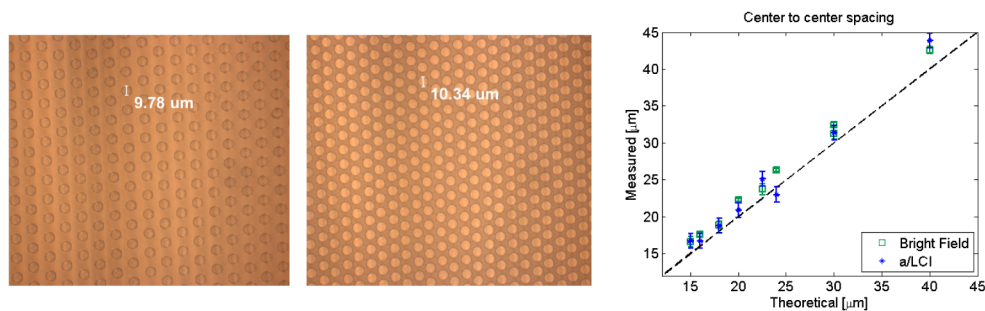


Fig. 2. Typical images of the fabricated mold under bright field illumination. (Left) Image of 'A' configuration sample with scattering features of nominally $10 \mu\text{m}$ diameter and $10 \mu\text{m}$ spacing. (Center) Image of 'B' configuration sample with scattering features of nominally $10 \mu\text{m}$ diameter and $5 \mu\text{m}$ spacing. Measurements shown on figure are from image analysis. (Right) Plot of correlation measurements of scatterer spacing (center to center) for image analysis of bright field images (green squares) and 2D a/LCI (blue stars). Theoretical values are based on fabrication mold parameters.

b. Phantom fabrication

Phantoms are constructed via soft lithography using polydimethylsiloxane (PDMS). The master mold for this procedure was created on a 4" silicon wafer by photolithography. The wafer was spin-coated with SU-8 photoresist and then exposed to UV light through a chrome-on-glass photomask. After being developed and washed in solvent, this exposure produced the desired mold features on the wafer. PDMS was degassed and then poured onto this mold, previously covered by a monolayer of hexamethyldisilazane (HMDS), before being cured at 70°C for a minimum of 2 hours. The resulting structures were then gently peeled off using forceps and affixed to No. 0 cover glass slides ($0.085 - 0.130 \text{ mm}$ nominal thickness) to create the light-scattering phantoms. Several different structures were fabricated, including regular and irregular arrangements. The regular phantoms consisted of hexagonally-packed circular features with two different spacing schemes: one where scatterers are spaced edge to edge by a distance equal to their diameter ('A' samples) and another where the edge to edge

spacing is half the diameter ('B' samples). For clarity, the center to center distances on the 'A' samples is twice the diameter while the center to center distances on the 'B' samples is 1.5 times the diameter. Figure 2 shows example images of the molds used to create the phantoms under bright field illumination for both 'A' and 'B' configurations.

These phantoms have light scattering properties similar to self-assembled monolayers (SAMs) of microspheres, which offer a high degree of radial and self-symmetry. While these are analogous to an ordered layer of cells, as could be found in the epithelium, the arrays are more highly ordered. Additional samples were fabricated using less regular arrangements. These will be presented below in detail. The ability to fabricate regular arrays of scatterers make these phantoms a logical basis for studying long range order using 2D a/LCI.

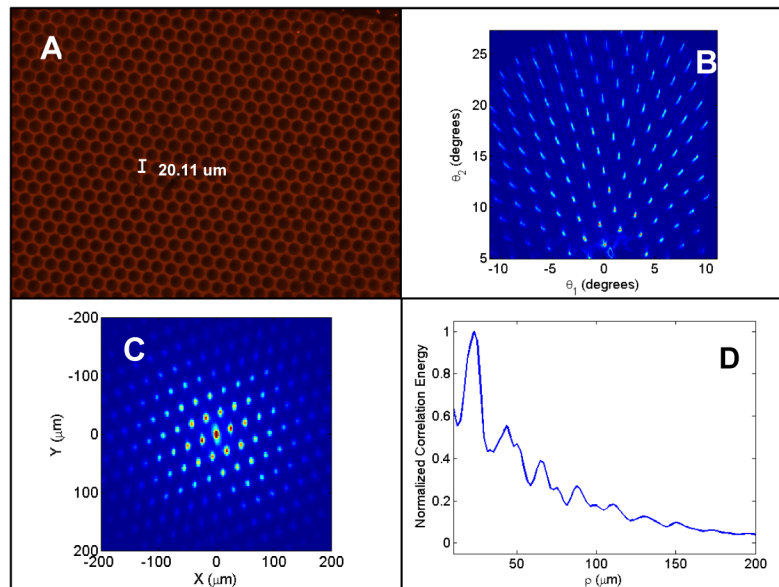


Fig. 3. (A) Bright field image of the 20 μm hexagonal packed phantom. (B) Scattering plane from the 20 μm SAM phantom collected via 2D a/LCI. (C) Correlation plane of the 20 μm SAM phantom. (D) Correlation of the 20 μm SAM phantom as a function of radial displacement.

3. Phantom characterization

We obtained light scattering measurements from the PDMS optical phantoms using a 2D a/LCI instrument with an beam diameter of 200 μm input to the sample. To analyze this information, autocorrelation distributions are constructed using 2D FT analysis. Analysis of the scattering from these phantoms provides accurate information about the spacing and distribution of individual elements within the phantoms. Typical data are shown for a scattering phantom with 20 μm nominal scatterer size and 3 μm spacing (Fig. 3(a)). The 2D a/LCI data are resolved by depth. To enable analysis, the depth plane corresponding to the phantom features is selected. The scattering distribution for the depth plane corresponding to the phantom features is shown in Fig. 3(b). Note that the information is specified as horizontal and vertical polar angles (θ_1 , θ_2) which facilitates Fourier analysis. The range of θ_1 is chosen to be symmetric about the origin but θ_2 is unidirectional, partly due to the use of a beam block to obscure specular reflection. We note that the symmetric nature of scattering distributions results in no loss of information with this choice [12]. The use of a beam block is possible here since the priority is long range correlation data which persists over large angular ranges, in contrast to analysis of Mie scattering in previous a/LCI studies where most useful information is localized near the origin. In these data distortion is seen towards the edges of

the imaged plane which are due to limitations of imaging a wide angular range using an imaging spectrometer.

The correlation distribution from the phantom (Fig. 3(c)) highlights the hexagonal packing of structural elements. When the 2D correlation is integrated azimuthally, the distance between peaks in the radial correlation energy matches the spacing of elements within the optical phantom (Fig. 3(d)). For the 20 μm scattering phantom, the measurement of $23.0 \pm 1.0 \mu\text{m}$ at the first peak in radial correlation energy is in agreement with the true spacing of 23.0 μm , the diameter of a circular element plus the inter-element spacing of 3.0 μm . Note that this spacing is different from the 'A' and 'B' configurations discussed above. We have included this additional sample to illustrate the presence of higher order peaks in the correlation energy, which are not as clear when the element spacing and size are integer/half-integer multiples. For the sample shown in Fig. 3, the peaks in the radial correlation energy displayed are accurate for up to four or more repeats of the sample elements, for example a distance of $90.8 \pm 2.1 \mu\text{m}$ is observed versus the true distance of 92.0 μm , resulting in only a 1.3% error. The measurements of the scattering phantom are presented in Table 1, along with measurements for several phantom geometries ranging from 8 to 20 μm scatterer size in both the 'A' and 'B' configurations. Figure 2 shows these measurements graphically. Both the image analysis and 2D a/LCI measurements show a linear relationship, producing R^2 values of 0.9961 and 0.9943 respectively compared to a best fit line. However, both measurements consistently overestimate the sizes such that the y-intercept of the fitted lines are non-zero, corresponding to 0.83 and 0.89 micron offsets for the image analysis and 2D a/LCI respectively.

Table 1. Comparison of correlation measurements via 2D a/LCI and image analysis of microscope images.

Sample (Diameter, Spacing)	Image Analysis (μm)	2D a/LCI (μm)	Percent Error
8A: 8 μm , 8 μm	17.6 ± 0.3	16.7 ± 1.0	5.1%
10A: 10 μm , 10 μm	22.3 ± 0.2	20.9 ± 1.0	6.3%
10B: 10 μm , 5 μm	16.6 ± 0.7	16.7 ± 1.0	0.6%
12A: 12 μm , 12 μm	26.3 ± 0.2	23.0 ± 1.0	12.5%
12B: 12 μm , 6 μm	18.9 ± 0.5	18.8 ± 1.0	0.5%
15A: 15 μm , 15 μm	32.5 ± 0.3	31.4 ± 1.0	3.4%
15B: 15 μm , 7.5 μm	23.7 ± 0.7	25.1 ± 1.0	5.9%
20A: 20 μm , 20 μm	42.6 ± 0.5	43.9 ± 1.0	3.1%
20B: 20 μm , 10 μm	31.3 ± 0.8	31.4 ± 1.0	0.3%

In addition to analyzing phantoms with well-defined structural features and hexagonal packing, we also sought to create phantoms that were more representative of the geometries seen for cells within epithelial tissues. Figure 4 shows an example of a phantom with rings of scatterers with 20 μm nominal diameter, arranged in rings that are approximately 100 μm in nominal diameter as one might find in crypts within colonic epithelium. Figure 4(a) shows a bright field image of the sample and Fig. 4(b) shows the 2D a/LCI pattern. Note that the features are not as easily identified in the a/LCI scan due to the increased complexity of the structure. However, upon 2D Fourier analysis of the scattering data, the resulting 2D correlation function (Fig. 4(c)) shows clearly identifiable features. These include a central peak occurring at approximately 20 μm in correlation length, corresponding to the scatterer diameter, a broader pedestal which is approximately 100 μm in correlation length, corresponding to the ring structure, and finally clear peaks along the directions of neighboring rings occurring at approximately 115 μm in correlation length revealing information on the long range order. Note that the sample structure is anisotropic with the spacing of the ring

structures varying with direction. We note that the pedestal, corresponding to the crypt like ring structure, is more clearly visible on the 2D correlation plot than the radially averaged plot, but in contrast the opposite is true for the ring to ring correlation peak, as seen in the correlation plot in Fig. 4(d).

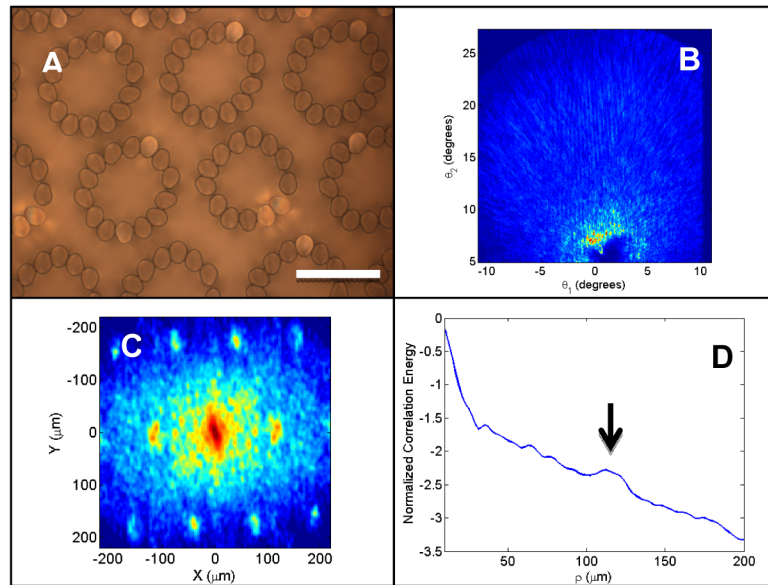


Fig. 4. (A) Bright field image of the crypt configuration scatterers (scale bar = 100 μm). (B) Scattering plane image collected via 2D a/LCI. (C) Correlation plane of for the crypt configuration phantom. (D) Correlation of the crypt configuration phantom as a function of radial displacement (log scale).

4. Discussion

We have presented and characterized a novel phantom for light scattering studies, created using soft lithography techniques. The phantoms enable controlled measurements of scatterers configured to exhibit long range order when measured with 2D a/LCI. The circular scatterers arranged in hexagonally packed configurations can be easily measured via simple analysis of Fourier transformed scattering data. Good agreement is seen between the structural measurements of the phantoms made with a/LCI and those acquired via quantitative image analysis of micrographs. We note a consistent trend where the ‘A’ configuration seems to produce slightly smaller measurements for a/LCI than via microscope. This may be due to the use of the same dimension for scatterer diameter and spacing, i.e. the edge to edge distance is the same as the scatterer diameter which may have caused aliasing in the FT.

Previous a/LCI studies using the 1D system characterized cell-to-cell correlations using micro-patterned substrates to adhere cultured cells in regular arrays [13]. This study enabled measurement of cellular structure and cell-to-cell correlation. However, the 1D a/LCI configuration required laborious alignment of the micropatterned substrate with the axis of the detected scattering plane. The 2D a/LCI method, on the other hand, measures long range correlation regardless of sample orientation. Further, the FT relationship between the scattered intensity and spatial correlation enables analysis of long range correlations [1].

The crypt configuration sample offers additional utility compared to the hexagonal packed scatterers in that organization is seen on multiple length scales, corresponding to the individual scatterer, the crypt like ring and the correlation between adjacent rings. The ability to measure correlations along multiple length scales has the potential to provide diagnostic information on tissue architecture, which could extend the sensitivity of a/LCI from disease at

the sub-cellular scale (cell nuclei) to the tissue scale. Further studies with normal and diseased epithelial tissues using 2D a/LCI will further explore this connection.

Acknowledgments

This work was supported by grants from the Coulter Foundation and the National Eye Institute 1R21 EY023451 and a Lord Foundation Grant to SKY for use of the Shared Materials Facility at Duke University.